Recent advances in perovskite oxide heterostructures of $La_{0.9}Sr_{0.1}MnO_3/SrNb_{0.01}Ti_{0.99}O_3$

Wang Cong, Jin Kui-Juan*, Guo Hai-Zhong, Lu Hui-Bin, Wang Can, He Meng, Yang Guo-Zhen

Beijing National Laboratory for Condensed Matter Physics, Institute of Physics, Chinese Academy of Sciences, Beijing 100190, People's Republic of China

To seek the inherent nature and potential applications of perovskite oxide heterostructures, great efforts have been made in the past few years. In this review paper, we summarize our systematic theoretical study on a variety of novel properties of the perovskite oxide heterojunctions, including the revealing of the physical origins behind the unusual positive magnetoresistance and the lateral photovoltage in $La_{0.9}Sr_{0.1}MnO_3/SrNb_{0.01}Ti_{0.99}O_3$ heterostructures. The theoretical model we present will be helpful for understanding the important role that the interface plays in determining the properties of the perovskite oxide heterostructures.

Key words: perovskite oxide heterostructures; positive magnetoresistance; lateral photovoltage; interface

CLC number : O482.5 Document Code : A

CONTENTS

I. INTRODUCTION

Perovskite oxides represent a class of materials with a remarkable range of fascinating and intrinsic physical functionalities, including high-temperature superconductivity and colossal magnetoresistance (CMR). These emergent properties are intimately related to the coexistence of competing nearly degenerate states which simultaneously couple to active degrees of freedom: charge, lattice, orbit, and spin states[1~3]. In particular, some emergent novel properties at the interfaces between different perovskite oxides in heterostructures have been revealed in respect that the charge and spin states are reconstructed at the interfaces and hence affect the electronic and magnetic properties of the entire system[4]. For instance, high-mobility electron gas was discovered between two insulating perovskite oxides $LaAlO_3$ and $SrTiO_3$[5]. Later, superconductivity[6] and magnetic effect[7] were also observed in this heterostructure. It was proposed that the interface effect is a crucial mechanism underlying those fascinating phenomena[8]. Following the emergence of a series of the novel properties in the perovskite oxide heterostructures, a theoretical understanding of the physical origin becomes fundamentally important.

In this review paper, we present our systematic theoretical study on novel properties of the oxide heterostructures. Based on the observation of an unusual positive magnetoresistance (MR) property in a kind of p-n heterostructures consisting of a n-type non-magnetic $SrNb_{0.01}Ti_{0.99}O_3$ (SNTO) and a p-type negative CMR material $La_{0.9}Sr_{0.1}MnO_3$ (LSMO)[9], a theoretical model related to the interface of the heterostructure was proposed to explain the origin of this positive MR property[10]. To obtain further insight, phase separation scenario[11] and spin current[12] were introduced to understand the dependence of MR magnetic field, temperature, bias voltage and composition in our self-consistent calculations, and excellent agreement between the calculated results and the experimental data was achieved[11,12]. Following the observation of an unusual lateral photovoltage (LPV) in the LSMO/SNTO heterostructure[13], we proposed that this lateral photovoltage was related to the evo-

Received date: 2010-08-30
*kjjin@aphy.iphy.ac.cn

lution and competition processes of the conventional lateral photovoltage and Dember effect induced lateral photovoltage[14]. Then two main physical origins for such an enhancement of LPV in the oxide heterostructures compared to that of the substrates were revealed[15].

II. RESULTS

A. Unusual positive CMR in oxide heterostructures

Since the discovery of CMR phenomena in mixed-valence manganites, much attention has been paid to materials and structures with remarkable magnetoresistance, such as various manganite films[16] and magnetic tunnel junctions (MTJ)[17], for potential applications in magnetic sensors and magnetic memory devices.

Different from the negative MR effect in most of these materials and structures, an unusual positive MR was discovered in low applied magnetic fields and at high temperatures in an epitaxial *p*-*n* heterostructure of LSMO/SNTO[9]. The LSMO/SNTO heterostructure was deposited using a computer-controlled laser molecular-beam epitaxy (LMBE) system using depositing $La_{0.9}Sr_{0.1}MnO_3$ with a thickness of 400 nm directly on $SrNb_{0.01}Ti_{0.99}O_3$ (001) at 630 °C using a XeCl pulsed laser (wavelength of 308 nm, duration of 20 ns, and repetition rate of 2 Hz). The laser energy density on the target surface was about 1 J/cm^2, and the oxygen pressure of 2×10^{-3} Pa was maintained throughout the deposition. The electrical and magnetic properties of the LSMO/SNTO *p*-*n* junctions were measured in the temperature range from 100 to 300 K. The magnetic field was applied perpendicularly to the interface and parallel to the current. The MR ratios, defined as $\Delta R/R_0$ ($\Delta R = R_H - R_0$) where R_H is the resistance in the applied magnetic field and R_0 is the resistance in zero field, were observed as large as 11 % in 5 Oe, 23 % in 100 Oe, and 26 % in 1000 Oe at 290 K; 53 % in 5 Oe, 80 % in 100 Oe, and 94 % in 1000 Oe at 255 K. To understand the physics of this unusual positive MR effect, we demonstrated a scenario in which the unusual positive MR effect was proposed as an interface effect, i.e., the creation of a space charge region near the interface with different electron filling in bands compared to that in the homogeneous region in LSMO[10].

The schematic of the measurement and the calculated energy band structure at a bias of −0.5 V of the LSMO/SNTO heterojunction were shown in Fig. 1(a) and (b)[11], respectively. In Fig. 1(b), $E_{\rm fn}$ is the Fermi level in the SNTO, $E_{\rm ip}$ is the bottom of conduction

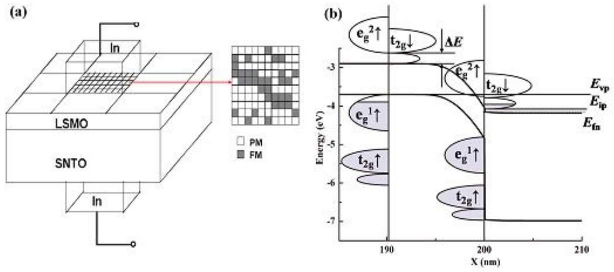

FIG. 1. (a) The schematic of the measurement on the LSMO/SNTO heterojunction. (b) The calculated energy band structure at a bias of −0.5 V with the electron and hole doping concentrations of 2.0×10^{20} cm^{-3} for SNTO and 4.0×10^{19} cm^{-3} for LSMO respectively at 255 K in LSMO/SNTO junction and the corresponding schematic DOS of the junction.

band of LSMO at the interface, and $E_{\rm vp}$ is the top of the valence band at the left boundary of LSMO, respectively. The physical origin of the positive MR at a given temperature has been revealed as the competition between the tunneling rates of electrons in the $e_{\rm g}^1\uparrow$ band to $t_{2\rm g}\downarrow$ band and that to $e_{\rm g}^2\uparrow$ band at the interface region of LSMO[10]. To gain further insight into this positive MR behavior, phase separation scenario[11] and spin current[12] were introduced to understand the dependences of MR with magnetic field, temperature, bias voltage and composition.

The percolation mode on the basis of the phase separation mechanism, which means the ferromagnetic metal phase and the paramagnetic insulator phase coexist at a given temperature, was used to interpret the negative CMR behavior around $T_{\rm c}$ in manganites[18]. Since the typical size of the ferromagnetic phase clusters (0.6∼1.1 μm[19]) is much smaller than the size of the electrode (0.5 mm), the electrode can cover a large area with many ferromagnetic and paramagnetic phases, as illustrated in Fig. 1(a). The resistance of the paramagnetic phase can be calculated from our model which was reported before[10], and the resistance of the ferromagnetic phase can be deduced from previous experiments[20]. Moreover, based on the percolation mode, the distribution of the ferromagnetic and paramagnetic phases at temperatures of 100, 150, 200, and 300 K is also obtained from Monte Carlo simulation[11]. Considering the parallel connection of the resistance in the ferromagnetic and paramagnetic phases, the resistance and magnetoresistance of LSMO/SNTO heterojunction can be obtained theoretically.

The experimental and theoretical MR dependences on magnetic field at temperatures of 100, 150, 200, and 300 K are shown in Figs. 2(a) and (b)[11], respectively. Fig. 2(c) shows the calculated MR as a function of temperature with magnetic fields of 0.1,

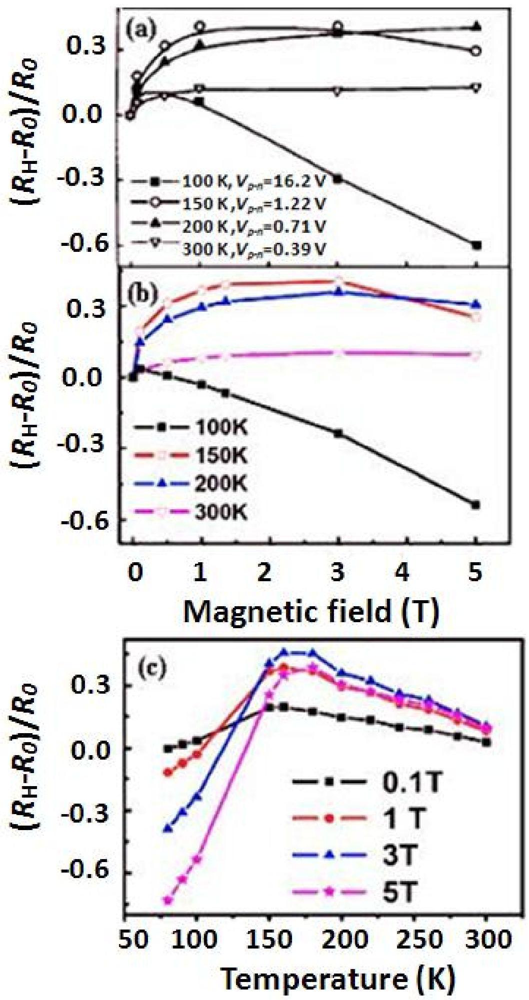

FIG. 2. (a) The experimental MR dependence on magnetic field at the temperature range from 100 to 300 K in LSMO/SNTO *p*-*n* junction. (b) The calculated MR dependence on magnetic field at the temperature range from 100 to 300 K in LSMO/SNTO *p*-*n* junction. (c) The calculated magnetoresistance as a function of temperature with the magnetic fields of 0.1, 1, 3, and 5 T, respectively.

1, 3 and 5 T, respectively. The MR behaves with a negative characteristic at low temperature of 100 K with large magnetic field and represents a positive MR property at the temperature range from 150 to 300 K with magnetic field below 5 T. The behavior of CMR at various temperatures is explained based on the phase separation scenario and positive MR mechanism as follows. At the temperature of 100 K, the effect of positive MR on the paramagnetic phase is greater than that of the negative one on the ferromagnetic phase at magnetic field smaller than 0.13 T. Thus, the total MR displays a positive characteristic in this magnetic field region. With the increase in magnetic field, the value of negative MR increases rapidly and the negative MR becomes dominated. At temperatures of 150 and 200 K, the MR is positive, and it reaches a maximum value and then decreases with the increase in magnetic field. At low magnetic field, the value of positive MR is larger than that of negative ones. Therefore, the total MR increases with magnetic field. With the further increase in magnetic field, the positive MR is a constant value due to the saturation of spin polarization, while the absolute value of negative MR still increases. Thus, the total MR decreases with further increase in magnetic field. Due to the much smaller proportion of the ferromagnetic phase with that of paramagnetic phase in 300 K, the contribution of negative MR to the total MR is very small, so that the total MR is positive under the magnetic field. Moreover, due to the saturation of spin polarization at higher magnetic field, the total MR is nearly a constant value with the increase in magnetic field.

To obtain the dependence of MR on bias and hole doping concentration with varied spin polarization, spin polarized current was employed in the transport calculation of the perovskite oxide *p*-*n* junction. The calculated distributions of the electric field intensity and carrier concentrations of the LSMO/SNTO heterostructure are given in Fig. 3(a) and (b)[12], respectively. Calculations for the tunneling spin currents were carried out at reverse bias by solving Schrödinger equation, and the MR ratios can be obtained through the tunneling spin currents. More details of the calculations can be found in Ref. 12.

Figure 3(c) displays the calculated MR value dependent on negative bias with varied spin polarizations at the temperature of 255K in the LSMO/SNTO $p-n$ junction. The corresponding experimental results are shown in Fig. 3(d). From the dependence of MR value on reverse bias with various spin polarization, it can be seen that with the increase of reverse bias, the value of MR increases to a maximum and then decreases swiftly. Furthermore, from the comparison of Fig. 3(c) and (d), it can be concluded that the spin polarization of the structure increases with magnetic field since the value of MR increases with both the spin polarization and the magnetic field, and the calculated results are in good agreement with experimental data. At a small negative bias under magnetic field, electrons in $e_g^1\uparrow$ band in the homogeneous region of LSMO can only tunnel to $t_{2g}\downarrow$ band that is partly lower than $e_g^2\uparrow$ band in the space charge region of LSMO. With the increase of negative bias, E_{vp} can equal or even exceed the bottom of $e_g^2\uparrow$ band. From the energy band structure shown in Fig. 1(b), it can be concluded that the electrons in $e_g^1\uparrow$ band have the probability of tunneling to both $t_{2g}\downarrow$ band and $e_g^2\uparrow$ band under magnetic field. The spin antiparallel tunneling causes a decrease of current, while the spin

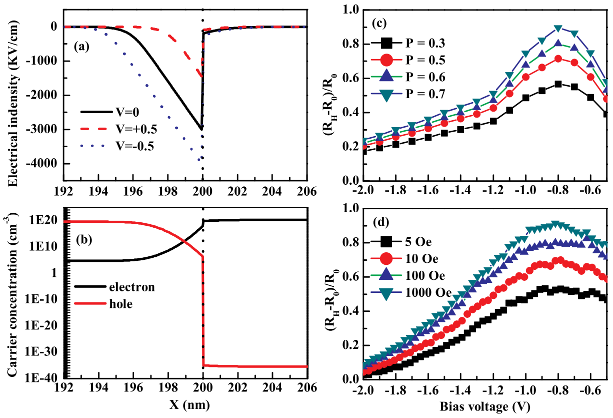

FIG. 3. (a) The distributions of the electric field intensity at various applied bias voltages at 300 K in the LSMO/SNTO heterostructure. (b) The distributions of the carrier concentrations of the LSMO/SNTO heterostructure at zero bias at 300 K. The vertical dotted line denotes the interface of the *p*-*n* junction. (c) The calculated results of MR value dependent on negative bias with the spin polarizations of 0.3, 0.5, 0.6, and 0.7 at the temperature of 255 K in the LSMO/SNTO junction. (d) The experimental data of MR value dependent on negative bias under the magnetic field of 5, 10, 100 and 1000 Oe at 255 K in LSMO/SNTO junction.

parallel tunneling causes an increase of current. At first, the current tunneling to $t_{2g}\downarrow$ band is larger than that to $e_g^2\uparrow$ band, so that the value of positive MR increases with bias. When the tunneling current of electrons from $e_g^1\uparrow$ band to $t_{2g}\downarrow$ band is equal to that to $e_g^2\uparrow$ band, the positive MR value reaches a maximum. With further increasing of negative bias, the current tunneling to $e_g^2\uparrow$ band increases more rapidly than that to $t_{2g}\downarrow$ band, so the positive MR starts to decrease with bias. Therefore, the competition between the current tunneling to $t_{2g}\downarrow$ band and to $e_g^2\uparrow$ band leads to the variation of positive MR value under applied negative bias. It can also be concluded that the spin polarization of conducting electrons increases with magnetic field, which leads to the increase of MR value with magnetic field, as a dependence of spin polarization of the system on magnetic field can be found from the comparison of calculated MR and experimental data shown in Fig. 3(c) and (d), respectively.

The large sensitivity of the MR to the magnetic field of the LSMO/SNTO heterostructure may meet the high desire for the application of a large MR ratio under low magnetic field and near room temperature. We believe that the employment of the spin current in our model has potential applications in designing MR-related devices in perovskite oxides.

B. Lateral photovoltage in perovskite oxide heterostructures

With a nonuniform irradiation on a *p*-*n* junction, an additional photovoltage parallel to the transverse photovoltage can be produced. This photovoltage is recognized as the lateral photovoltage[24]. According to the conventional LPV theory[25~28], in the nonuniformly irradiated *p*-*n* junction, the photo-induced electrons and holes near the irradiation center are swept into *n* and *p* type sides by the built-in field, and diffuse out of the irradiation regions in the *n* and *p* type sides, respectively[28]. Thus, the electric potential near the irradiation center is higher than that far from the center on the *p*-type side, while it is lower on the *n*-type side.

However, an unusual LPV phenomenon was recently observed in the LSMO/SNTO heterojunction[13]. Its fabrication conditions have been described in the preceding section. A small area of 0.5 mm diameter on the *p*-LSMO surface was irradiated by a 308 nm XeCl excimer laser beam (pulse width of 20 ns, irradiated energy of 0.15 mJ, and repetition rate of one pulse every 5 min to avoid the heating effect). The LPVs were measured and recorded by a sampling oscilloscope of 500 MHz

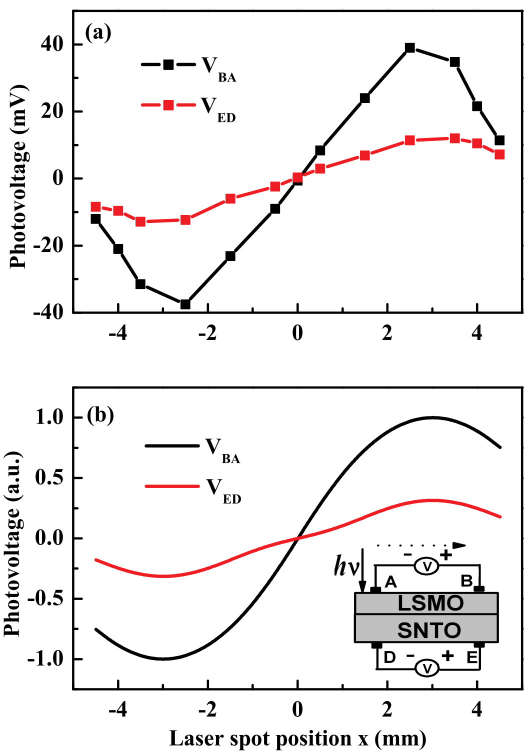

FIG. 4. (a) The experimental unusual LPV in the LSMO/SNTO heterostructure; (b) The calculated LPV in the LSMO/SNTO heterostructure. The lower inset shows the schematic setup for LPV measurement.

terminated into 1 MΩ at ambient temperature. Especially, the electrodes were always kept in dark to prevent the generation of any electrical contact effect. Our observation challenged the conventional LPV explanation, since the photo-induced electric potential near the irradiation center on the two sides of the p-n junction are both higher than those far from the irradiation center on the p and n type sides, respectively. Therefore, Dember effect[29] was introduced in Ref. 15 to qualitatively explain the unusual lateral LPV in the oxide heterostructure. Dember effect, which is induced by the difference of carriers (holes and electrons) diffusion coefficients, has been widely studied on many semiconductor surfaces and applied in producing terahertz (THz) rays[30~32]. The larger LPV we discovered in oxide heterostructures than that in the bulk materials suggests some potential applications of the Dember effect in oxide heterostructures. Thus, the theoretical investigation on the dynamic process of LPV in oxide heterostructures, which can describe both the conventional and the unusual LPV effects, was carried out[14].

A unified description of the unusual LPV process was presented by solving the two-dimensional (2D) time-dependent drift-diffusion equations consisting of Poisson equation and the carrier continuity equations. More details of the calculations can be found in Ref. 14.

Figure 4(a)[14] shows the measured V_{BA} and V_{ED} dependence on laser position in the LSMO/SNTO heterojunction, where V_{BA} denotes the peak LPV between the indium electrodes A ($x = -3$ mm) and B ($x = 3$ mm) on the p-LSMO side, and V_{ED} denotes the peak LPV between the indium electrodes D ($x = -3$ mm) and E ($x = 3$ mm) on the n-Si side. Compared with Fig. 4(a), the calculated LPVs in the LSMO/SNTO heterojunction shown in Fig. 4(b) are in good agreement with the experimental results.

The thermal effect was ignored in the calculation, since we believed that the thermal effect is much smaller compared with the photon effect based on the phenomena we observed. First, if the thermoelectric effect dominated the process, with the thermal gradient, holes on LSMO side and electrons on SNTO side with opposite charge polarities should both diffuse toward the cooler region far from the laser spot, which should cause the LPV on LSMO being reverse to that on SNTO, and this is not the case we observed. Moreover, no signal was observed when the $SrTiO_3$ single crystal was irradiated by 532 or 632.8 nm laser with the photon energy being less than the band gap of $SrTiO_3$.

The calculated electric potential distributions in the LSMO/SNTO heterostructure with varied laser pulse

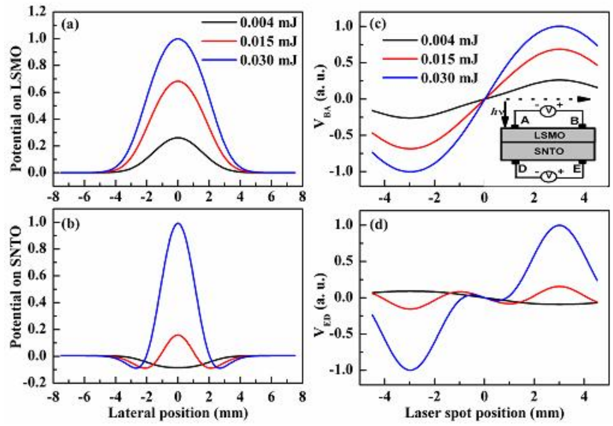

FIG. 5. The electric potential distributions near the irradiation center of the LSMO/SNTO heterostructure with varied irradiation laser pulse energies (0.004, 0.015, 0.030 mJ) (a) on the LSMO side and (b) on the SNTO side. The calculated LPVs of the LSMO/SNTO heterostructure with varied irradiation laser pulse energies (0.004, 0.015, and 0.030 mJ) (c) on the LSMO side and (d) on the SNTO side. The inset in Fig. 5 (c) shows the schematic setup for LPV measurement.

energies of 0.004, 0.015, and 0.030 mJ are shown in Fig. 5(a) and (b)[14]. With the increase of laser pulse energy, the value of the electric potential on the LSMO side becomes larger. With the laser pulse energy lower than 0.015 mJ, the trends of electric potential distribution on the two sides of the p-n junction are inverse to each other, while they turn to be the same with each other when the laser pulse energy is higher than 0.015 mJ.

Figure 5(c) and (d)[14] shows the calculated LPVs on two sides of the LSMO/SNTO heterostructure with varied laser pulse energies of 0.004, 0.015, and 0.030 mJ. As shown in Fig. 5(d), the calculated LPV on the n-type side exhibits a laterally modulated behavior with the laser pulse energy of 0.015 mJ, and the corresponding experiment is highly expected. This laterally modulated LPV effect can be explained by the competition between the Dember and the conventional LPV processes. Under this critical laser pulse energy, the Dember effect and the conventional LPV effect are comparable to each other and both affect the LPV all over the junction.

In the region near the irradiation center (−2.0 mm, 2.0 mm) where the carrier density is high owing to the strong laser pulse irradiation, the Dember effect is stronger than the conventional LPV effect, as shown in Fig. 5. Thus, in this region, the farther the position is away from the irradiation center, the smaller electric potentials are on both sides. While in the region far away from the irradiation center (2.0 mm, 7.5 mm) and (−7.5 mm, 2.0 mm) where the carrier density is low, the Dember potential is weak, as shown in Fig. 5.

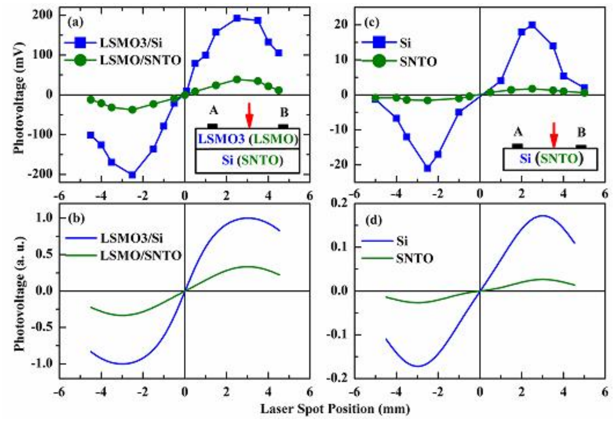

FIG. 6. The experimental (a) and theoretical (b) LPVs of the LSMO side in the LSMO/SNTO denoted by the green curve and $La_{0.7}Sr_{0.3}MnO_3$/Si denoted by the blue curve; the experimental (c) and theoretical (d) LPVs of SNTO denoted by the green curve and Si denoted by the blue curve. The photovoltage denotes the peak value of LPV between the indium electrodes A ($x = -3$ mm) and B ($x = 3$ mm). The inset shows the schematic setup for the LPV measurement.

Consequently, the conventional LPV effect is the main contributor to the LPV. Therefore, our calculated results unified the description of the conventional LPV and the Dember effect into the drift-diffusion equations.

Through the above theoretical investigation, two main physical origins for such an enhancement of LPV in the oxide heterostructures compared to that of the substrates were revealed[15]. Fig. 6 (a) exhibits the experimental LPVs of LSMO side in the LSMO/SNTO and $La_{0.7}Sr_{0.3}MnO_3$/Si (LSMO3/Si) heterostructures, while Fig. 6(b) depicts the experimental LPVs of SNTO and Si substrates. From Fig. 6(a) and (b), it can be seen that a one-order-of-magnitude enhancement of the LPVs was observed, as compared with those of the substrates. Our calculated results for LPVs on the LSMO side in LSMO/SNTO and LSMO3/Si heterostructures are shown in Fig. 6(c). The calculated LPVs on SNTO and Si substrates are displayed in Fig. 6(d).

Firstly, we find that the Dember-effect-induced LPV of the p-type material is larger than that of the n-type material with the same carrier concentration. As illustrated in Fig. 7(a), we calculated the Dember effect-induced LPVs of the p-type material and n-type material with the same carrier concentration of 1×10^{17} cm^{-3}. It can be seen that the LPV of the p-type material is almost twice as large as that of the n-type material. This can be totally attributed to the difference between the mobilities of electrons and holes.

Secondly, we found from our calculations that the

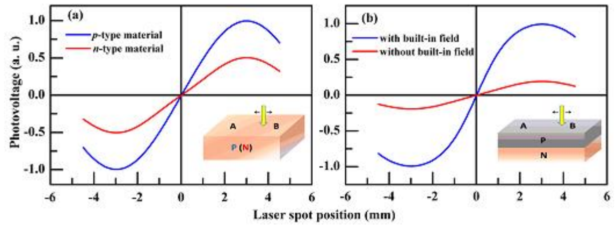

FIG. 7. (a) The calculated LPVs between the electrodes A ($x = -3$ mm) and B ($x = 3$ mm) in the same material with different doping type. The blue and red curves denote the LPVs in the p-type and n-type material, respectively. The inset exhibits the schematic setup. (b) The blue and red curves denote the calculated LPVs between the electrodes A ($x = -3$ mm) and B ($x = 3$ mm) in the same heterostructures with built-in field and without built-in field, respectively. The lower inset exhibits the schematic setup.

built-in electric field at the interface between the thin film and the substrate also plays an important role in the LPV effect. To reveal the effect of the built-in electric field, we assumed that the potential difference between the p-type region and the n-type region was zero and 0.52 V for the structure without and with the built-in electric field in our self-consistent calculations, respectively. Fig. 7(b) shows the calculated LPVs for the heterostructure with and without the built-in electric field denoted by the blue curve and the red curve, respectively. From Fig. 7(b), it can be estimated that the heterostructure with a small built-in field of 0.52 V can produce a five times larger LPV than that of the heterostructure without the built-in field. When heterostructures are irradiated by the laser with the photon energy larger than the energy gaps of both the p-type side and n-type side, electron-hole pairs are produced in these structures. For the structure with the built-in electric field, the photo-generated electron-hole pairs can be separated by the built-in electric field. Thereby, the photo-generated holes are swept into the p-type layer, and the potential of the irradiation region is raised relative to the situation without the built-in electric field. Hence, the Dember effect-induced LPV for the structure with the built-in electric field is enhanced compared to the one without the built-in electric field. The combination of the above two mechanisms can well explain the one-order-of-magnitude enhancement of the LPV in the perovskite heterostructures.

III. SUMMARY

The discovery of the positive MR effect in the LSMO/SNTO heterostructure has inspired our theoretical exploration on its mechanism. A model related to interface effect has well explained the positive CMR features with bias voltage and composition. Phase separation and spin current were also introduced to interpret the MR behaviors with the variation of magnetic field, temperature, and bias voltage in our self-consistent calculations. Furthermore, an unusual LPV effects in this heterostructure were observed, and the evolution and competition processes of the conventional and Dember LPV effect was revealed theoretically. Two origins for such an enhancement of LPV in the oxide heterostructures compared to that of the substrates were revealed. Such progress should improve our understanding on the physics in oxide heterostructures and be helpful for the designing of novel devices in further functionally optimizing.

ACKNOWLEDGMENTS

The authors acknowledge the financial support from the National Natural Science Foundation of China and the National Basic Research Program of China.

REFERENCES

[1] Salamon M B, Jaime M. *Rev. Mod. Phys.*, 2001, **73**: 583
[2] Liu J M, Wang K F. *Progress in Physics*, 2005, **25**: 82
[3] Dong S, Liu J M. *Progress in Physics*, 2010, **30**: 1
[4] Dagotto E. *Science*, 2007, **318**: 1076
[5] Ohtomo A, Hwang H Y. *Nature*, 2004, **427**: 423
[6] Reyren N, Thiel S, Caviglia A D, *et al. Science*, 2007, **317**: 1196
[7] Brinkman A, Huijben M, *et al. Nat. Mater.*, 2007, **6**: 493
[8] Huijben M, Brinkman A, Koster G, *et al. Adv. Mater.*, 2009, **21**: 1665
[9] Lu H B, Dai S Y, *et al. Appl. Phys. Lett.*, 2005, **86**: 032502
[10] Jin K J, Lu H B, Zhou Q L, *et al. Phys. Rev. B*, 2005, **71**: 184428
[11] Hu C L, Jin K J, Han P, *et al. Appl. Phys. Lett.*, 2008, **93**: 162106
[12] Hu C L, Jin K J, Han P, *et al. Solid State Commun.*, 2009, **149**: 334
[13] Jin K J, Zhao K, Lu H B, *et al. Appl. Phys. Lett.*, 2007, **91**: 081906
[14] Liao L, Jin K J, Ge C, *et al. Appl. Phys. Lett.*, 2010, **96**: 062116
[15] Ge C, Jin K J, Lu H B, *et al. Solid State Commu.* 2010, **150**: 2114
[16] Haghiri-Gosnet A M, Renard J P. *J. Phys. D: Appl. Phys.*, 2003, **36**: 127
[17] Mitra C, Raychaudhuri P, Dorr K, *et al. Phys. Rev. Lett.*, 2003, **90**: 17202
[18] Moreo A, Yunoki S, Dagotto E. *Science*, 1999, **283**: 2034; Moreo A, Mayr M, Feiguin A, Yunoki S, Dagotto E. *Phys. Rev. Lett.* 2000, **84**: 5568
[19] Zhou Q L, Jin K J, Lu H B, *et al. Appl. Phys. Lett.*, 2007, **90**: 032508
[20] Urushibara A, Moritomo Y, Arima T, Asamitsu A, Kido G, Tokura Y. *Phys. Rev. B*, 1995, **51**: 14103; Tovstolytkin A, Pogorily A, Vovk A, Podyalovskii D, Lezhnenko I, Matviyenko A. *J. Magn. Magn. Mater.*, 2004, **272**: 1839
[21] Qiu J, Jin K J, Han P, Lu H B, *et al. Europhys. Lett.*, 2007, **79**: 57004
[22] Han P, Jin K J, Lu H B, Zhou Q L, Zhou Y L, Yang G Z. *Appl. Phys. Lett.*, 2007, **91**: 182102
[23] Zhou Q L, Jin K J, Lu H B, *et al. Europhys. Lett.*, 2005, **71**: 283
[24] Wallmark J T. *Proc. IRE.*, 1957, **45**: 474
[25] Lucovsky G. *J. Appl. Phys.*, 1960, **31**: 1088
[26] Groden C M, Richards J A. *Solid-State Electron.*, 1968, **11**: 997
[27] Groden C M, Richards J A. *Solid-State Electron.*, 1969, **12**: 813
[28] Amari S. *J. Phys.*(France), 1991, **1**: 1669
[29] Pankove J I. *Optical Processes in Semiconductors*, New Jersey, Prentice-Hall, Englewood Cliffs, 1971
[30] Gu P, Tani M, Kono S, Sakai K, Zhang X C. *J. Appl. Phys.*, 2002, **91**: 5533
[31] Dekorsy T, Auer H, Bakker H J, Roskos H G, Kurz H. *Phys. Rev. B*, 1996, **53**: 4005; Dekorsy T, Pfeifer T, Kütt W, Kurz H. *ibid.*, 1993, **47**: 3842
[32] Ascazubi R, Wilke I, Kim K J, Dutta P. *Phys. Rev. B*, 2006, **74**: 075323

钙钛矿氧化物异质结的研究进展

王　聪，金奎娟，郭海中，吕惠宾，王　灿，何　萌，杨国桢

北京凝聚态物理国家实验室，中国科学院物理研究所，北京 100190

摘要： 在过去几年中，为了研究钙钛矿氧化物异质结的物性和潜在的应用前景，我们进行了许多探索。在本文中，我们总结了对钙钛矿氧化物异质结一些物理性质的理论描述，揭示了$La_{0.9}Sr_{0.1}MnO_3/SrNb_{0.01}Ti_{0.99}O_3$异质结中发现的正磁电阻效应和横向光电效应的物理起源。我们提出的理论模型将有助于理解界面对钙钛矿氧化物异质结各种性质的影响。

关键词： 钙钛矿氧化物异质结；正磁电阻；横向光电效应；界面